DOI: 10.61782/fa.2025.0478

FORUM ACUSTICUM EURONOISE 2025

INJECTION MOULDED LOCALLY RESONANT RINGS FOR VIBRATION MITIGATION IN PIPES

K. Steijvers[*1,2] **U. Arasan**[1,2] **C. Claeys**[2,3]
L. Van Belle[2,3] **E. Deckers**[1,2]

[1.] KU Leuven, Campus Diepenbeek, Department of Mechanical Engineering, Wetenschapspark 27, 3590 Diepenbeek, Belgium
[2.] Flanders Make@KU Leuven
[3.] *KU Leuven, Department of Mechanical Engineering, Celestijnenlaan 300B box 2420, 3001 Heverlee, Belgium*

ABSTRACT

Locally resonant metamaterials (LRMs) are promising lightweight solutions for targeted vibration attenuation, achieved by incorporating resonant elements on a sub-wavelength scale into a host structure. However, manufacturability limitations form a major hurdle in their industrial adoption. Additive manufacturing offers design versatility but lacks industrial-scale throughput, while high-throughput techniques such as laser cutting or punching of resonators often require labor-intensive assembly steps to create the LRM. Furthermore, manufacturing-induced deviations in geometry and material properties can significantly impact the vibro-acoustic LRM performance, often necessitating multiple design iterations. This study addresses these challenges by proposing the high-throughput injection moulding process while accounting for process-induced influences on the LRM performance using a process simulation-informed design workflow. Injection moulding enables robust and large-scale manufacturing, whereas dedicated process simulations allow incorporating manufacturing process influences in the vibro-acoustic performance predictions. This work therefore presents the design, manufacturing and experimental validation of an injection moulded LRM demonstrator to treat a noise radiation problem around a targeted vibration mode of an aluminum pipe. The achieved vibration reduction and good agreement with the model-based predictions demonstrate the strong potential of injection moulding for the mass-manufacturing of LRMs with targeted performance.

Keywords: Locally resonant metamaterials, Injection moulding, Demonstrator

1. INTRODUCTION

The machine and transportation industries are increasingly adopting lightweight design to reduce material use, energy consumption and environmental impact. However, the resulting lightweight structures often come with deteriorated noise and vibration characteristics, impacting our health and well-being. As

[*] ***Corresponding author***: kristof.steijvers@kuleuven.be

a solution, locally resonant metamaterials (LRMs) are currently investigated [1]. They allow for targeted frequency zones with strong vibration attenuation, so-called stop bands. These resonance-based stop bands result from the addition of resonant elements on or into a flexible host structure on a sub-wavelength scale [2].

LRMs are typically composed of periodic assemblies of identical unit cells (UC). Although periodicity is not strictly necessary for resonance-based stop bands, this facilitates the use of periodic structure modelling to predict wave propagation and stop bands early in the design stage. Dispersion curves are typically calculated from a finite element (FE) model of the representative periodic UC, combined with Bloch-Floquet periodicity boundary conditions [2].

Building upon these prediction tools, the potential of LRMs has been widely explored and demonstrated through many conceptual LRM realizations. Nevertheless, the manufacturing of LRMs is found to be challenging since the integration of resonant elements often leads to geometrically intricate geometries. Consequently, additive manufacturing (AM) has become a strong enabler in the manufacturing of LRMs. However, additive manufacturing techniques currently do not reach the throughput for commercial applications [3]. In attempts to transition towards more mass-manufacturing suited processes, laser cutting and milling have been used to produce separate resonators. Moreover, LRM structures have been manufactured using thermoforming and punching [4], requiring a post-production milling or bending step to realize the resonators. Recently, the injection moulding (IM) has been proposed for the manufacturing of resonators [5] [6]. This process comes with low costs when used for mass-manufacturing and allows achieving lower process variability in terms of dynamic LRM response compared to AM [5].

Besides the difficulties to manufacture LRM geometries, manufacturing processes also affect their geometry and material properties. Consequently, the final LRM geometry and material properties often deviate from the initial design, leading to off-design LRM performance. In case of AM, large deviations in the material properties together with anisotropy and geometric inaccuracies have led to off-design LRM stop bands [4]. In forming and bending processes, the stiffness and local density of the sheets is strongly affected by the difficult to control local thinning during forming. These effects significantly affect the resonator eigenfrequencies and, consequently, the resulting stop band. To achieve the desired LRM performance after manufacturing, design and material property updating is currently performed in iterative design steps. In case of the IM process, dedicated IM process simulations have been proposed to predict and account for process influences during the LRM design phase [7]. It is shown that for three different resonator geometries, manufactured in two materials, incorporating IM process simulations in the LRM design flow significantly improves the eigenfrequency predictions.

In view of practice-oriented solutions, LRMs have been often demonstrated as add-on resonators or resonator patches which can be applied to existing host structures. This is often more appealing to industry since it allows for LRM demonstration of existing products and machinery. For example, laser-cut resonators have been manufactured and manually glued to plates, and pipes [8] in academic demonstrators. Similar approaches have been reported to attach resonators manufactured with IM in [5].

Although successful IM mass-manufacturing of resonators with reduced off-design performance has been demonstrated, prior work has focused mainly on basic resonator geometries. This study advances the state-of-the-art by leveraging IM together with process simulation-informed LRM performance predictions to realize and validate a mass-manufacturable ready-to-use LRM solution for vibration mitigation in pipes. This allows to align the envisaged performance during LRM design and the as-manufactured performance and so reduces possible design iterations. As a demonstrator case, a aluminum tube similar to the one used in [8] is selected for targeted vibration attenuation around a dominant radiating mode. To facilitate LRM assembly, a snap-fit connection is integrated.

2. PROBLEM DESCRIPTION

The demonstrator targets an acoustically relevant ovalling mode in an aluminum pipe, inspired by [8]. An experimental modal analysis (EMA) is performed for modal identification and FE-model updating.

2.1 Experimental modal analysis

An impact hammer test is conducted to experimentally characterize the modal behavior of the pipe. To this end, the pipe is divided into a regular grid of 88 measurement points. The grid consists of 11 measurement points along the pipe's length, which are axially patterned 8 times around the circumference leading to a 45 degree shift between each measurement array. The pipe is suspended

in a free-free configuration and excited at each point using a PCB 086C03 modal hammer in a roving hammer sequence. The radial acceleration response is captured in measurement point 1 (0°, 0 mm length) and 29 (45°, 600 mm length) using two PCB ICP lightweight accelerometers. The point-to-point FRFs are calculated over 5 averages in Siemens Simcenter Testlab using the H_v approach. To avoid leakage, an exponential decaying window is applied to the excitation signal while a Hanning window is applied to the response signal.

2.2 Numerical eigenmode calculations

In order to accurately predict the LRM performance, a representative numerical host structure model is desired. To this end, a structural dynamic FE model of the host structure is created in Siemens Simcenter to calculate both the undamped eigenfrequencies and the acceleration response under force excitation. Specifically, a quadratic CQUAD8 shell mesh with an element size of 10 mm is applied to the pipe's midsurface. The pipe dimensions and mass are measured and listed Table 1. The pipe's real eigenfrequencies and forced response are calculated over a frequency range of 50-1200 Hz. For the latter, a normal unit force is applied at the first measurement point location, and the acceleration response is measured at all other measurement points. The predicted eigenfrequencies and forced response are compared to the experimentally determined modal frequencies and FRFs, whereafter the Young's modulus of the aluminum (69 GPa) is updated to the value of Table 1 to obtain good agreement between the numerical eigenfrequency of the first ovalling mode and the corresponding experimental value.

Table 1: Main dimensions and material properties of the targeted pipe host structure.

Length [mm]	1002	Young's Modulus [GPa]	81.8
Outer diameter [mm]	100.25	Density [kg/m^3]	2711
Wall thickness [mm]	2	Poisson ratio [/]	0.33
Mass [g]	1742.4		

Comparing the experimentally and numerically obtained FRFs (Figure 1a), three eigenfrequencies are identified in the frequency range under 1000 Hz. Figure *1*b, presents an overview of the FE-based real eigenmodes and the modal displacements obtained through the EMA at the peak frequencies. For the first frequency of 582 Hz, the ovalling and torsional mode are present, both of which were also identified from the EMA deformation pattern around 581 Hz. At 627 Hz, an ovalling pattern is observed, varying along the axial direction, in superposition with the first pipe bending mode. A similar modal deformation is observed in the EMA at approximately 620 Hz. Around 825 Hz, both the simulation and EMA show a similar out-of-plane behavior of higher order.

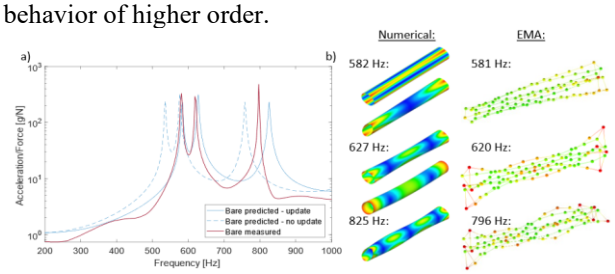

Figure 1: a) Comparison of the experimentally obtained and numerically predicted FRF of the bare pipe, b) numerically obtained real eigenfrequencies and experimentally obtained model displacement patterns at the determined resonance frequencies.

3. IDEALIZED METMAMATERIAL DESIGN

To design an LRM for targeting the first ovalling tube mode, both the LRM's vibro-acoustic performance and the IM manufacturability must be taken into account. Therefore, an idealized LRM design is optimized for a suitable eigenfrequency and hence stopband location, together with a maximized Modal Effective Mass (MEM) to increase the stop band width [2]. For three different designs resulting from the optimization, the IM manufacturability is assessed separately in Section 4.

3.1 Snap-fit ring concept

For the LRM design, eight resonant elements will be used, placed over each 45 degrees of the pipe circumference, in accordance with [8]. Whereas in this work the resonators have been manually glued to the host structure, a punched out add-on ring shaped concept has been shown in [4]. These rings allow to assemble multiple resonators simultaneously which reduces the risk op resonator misalignments, which potentially influence the final LRM performance. However, the resonator masses were still glued manually, hindering cost-effective series production. Building upon these studies, the proposed LRM in this work consists of two

identical ring sections with each four evenly distributed integrated resonators as illustrated in Fig. 2a. The ring sections can be assembled around the pipe using a snap-fit mechanism to form a closed ring. This simplifies LRM assembly by eliminating additional components. Furthermore, by moulding only half a ring at a time, the required mould size, melt volume and clamping force can be reduced, reducing the overall cost. As a result, the moulded product is ready-to-use, requiring no additional components for LRM assembly.

3.2 Resonator tuning and optimization

To create the resonance based stop band, an often-used cantilever beam type resonator is selected and adapted for integration on the ring base, targeting the first out-of-plane eigenmode. Fig. 2a,b show the design dimensions and the targeted first flexural eigenmode for a clamped ring circumference. The parameterized resonator dimensions are optimized towards a maximum MEM for the targeted eigenmode. The frequency tuning range was set around the ovalling frequency of the tube between 560-600 Hz, still allowing for a small misalignment to increase the design freedom. An exact tuning is in this stage redundant since the design will later still be tailored for IM manufacturing. Parameter ranges are set for the eight main resonator dimensions (Table 2). For these ranges, specific IM design rules are already accounted for. For example, wall thicknesses are kept under 4 mm to prevent voids caused by high shrinkage. Moreover, X_{Mass} is already set equal to X_{Leg} to facilitate filling during IM manufacturing. Lastly, the thickness of added ribs should not exceed 60% of the base structure thickness. In case the resonator is seen as a pure rib, the Y_{Leg} parameter would be highly restricted. However, the resonator is not a typical rib which is attached to the base structure over the entire rib length, therefore, this rule is not already incorporated. The selected material is ABS NOVODUR P2H-AT from INEOS (E = 2240 MPa, ρ = 1050 kg/m^3 , ν = 0.4). The optimization is performed using the hybrid adaptive SHERPA algorithm in Siemens Simcenter HEEDS across 400 designs. The objective function is formulated as follows:

Maximize MEM,

Subjected to:

$$560\ \text{Hz} \leq F_1 \leq 600\ \text{Hz}$$

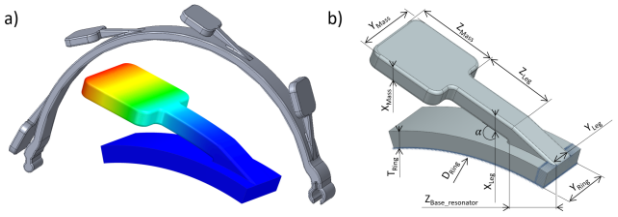

Figure 2: a) Conceptual LRM ring section with snap-fit mechanism, b) main dimensions of the LRM ring and resonator, c) targeted first out-of-plane eigenmode.

Three designs with high MEM are selected and will be evaluated for manufacturability in the following section. Table 2 lists the obtained dimensions, eigenfrequency and MEM for these designs. For all three designs, the resonator dimensions Y_{Mass} and Z_{mass} are maximized, as expected from the objective. The main differences between the designs relate to the resonator angle α, the cantilever beam length Z_{Leg} and the cantilever beam width Y_{Leg}. For design 2, the high MEM is obtained due to the high value of Y_{Leg}, whereas both the MEM and Y_{Leg} are smaller in design 3. Comparing design 2 to design 1, the steeper resonator angle in design 1 leads to only a minor difference in performance. Although design 2 offers the best MEM, it is the further away from the targeted ovalling eigenfrequency at 582 Hz.

Table 2: Baseline, min and max value of the design parameters for the optimization, followed by the obtained dimensions, eigenfrequency and MEM for the three selected designs.

Parameter	Baseline	Min	Max	Design 1	Design 2	Design 3
Y_{Ring}	8	4	10	10	10	10
$Z_{Base\_resonator}$	7	3	10	7	10	8
α	95	85	100	95	85	95
Z_{Leg}	18	10	25	17	17	14
X_{Leg}	3	2	3.5	3	3	3
Y_{Leg}	6	3	Y_{Ring}-1	8	8	5
X_{Mass}	X_{Leg}	-	-	3	3	3
Y_{Mass}	9	Y_{Leg}+3	14	14	14	14
Z_{Mass}	8	8	14	14	14	14
D_{Ring}	100.5	-	-	100.5	100.5	100.5
T_{Ring}	3	-	-	3	3	3
			Mode 1 [Hz]	570.1	568.5	575.6
			MEM [g]	0.69	0.7	0.62

4. LRM MANUFACTURABILITY AND MOULD

In this section, the idealized design is further assessed and tailored for IM manufacturing by taking into account

IM related process effects such as the volumetric shrinkage. The optimal resonator design is selected and the mould design and LRM manufacturing are explained.

4.1 Manufacturability assessment of the resonator

The IM process requires specific design guidelines to enhance mouldability and avoid defects such as sink holes, part warpage and internal stresses. These effects relate to the filling, packing and cooling steps of the IM process. During the filling stage, a speed controlled forward motion of the screw ensures precise injection. When the mould cavity is almost filled, the process transitions from speed to pressure regulation at the switch-over point. From this point, a defined packing pressure is maintained at the back of the screw to fill the remainder of the cavity and compensate for material shrinkage during part solidification. Here, the available packing time strongly depends on the part solidification, thin sections like the resonator leg might solidify rapidly, hindering material entrance in thicker part sections such as the resonator mass. When the packing is finalized, the screw retracts, preparing the next shot of material while the part continues to cool.
To predict the filling, solidification and shrinkage of the resonator, commercial IM simulations are used [7]. The process settings are set to rule of thumb starting values. More specifically, the injection speed is set to 40 cm^3/s and a packing pressure is held for 10 seconds at a level of 80% of the maximum filling pressure. The melt and mould temperature are set to 240 °C and 60 °C, respectively, in accordance with the material datasheet. The resulting volumetric shrinkage and solidification time are assessed for the three resonator geometries. The volumetric shrinkage is used to compare the designs' sensitivity for sink marks, while the solidification time provides an estimate of the available packing time.

4.2 Resonator mouldability

Fig. 3 illustrates the maximum volumetric shrinkage and molten core at the time step that the first design has a fully solidified cross section, after 17 seconds of cooling. Design 1 and 2 exhibit higher volumetric shrinkage at the resonator base compared to design 3, which is attributed to the larger Y_{Leg}. This indicates a higher risk of sink marks after manufacturing. In design 3, the risk of sink marks is reduced at the expense of a lower MEM due to the lower $Y_{Resonator}$ parameter. From the molten core values, the resonator arm of design 3 freezes around 17 seconds, while design 1 and 2 still have a molten connection between the ring and the resonator mass. Therefore, design 1 and 2 allow for longer packing time, as compared to design 3. However, 17 seconds is already longer than the value used in practical moulding given the typical small gates used for the overall part melt entrance, causing the gate freezing time to be the main bottleneck for the packing phase. As a result, the difference in $Y_{Resonator}$ will not impact the filling of the resonator mass significantly, which can also be concluded from the similar shrinkage values in the resonator mass. Based on these considerations and outcomes, design 3 is selected as the final resonator geometry.

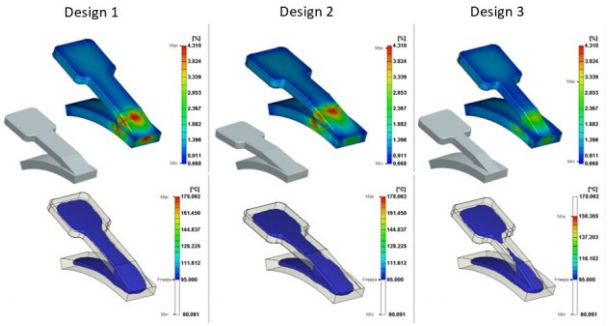

Figure 3: Volumetric shrinkage [%] (top) and molten core [°C] (bottom) after 17 seconds for the three selected designs.

4.3 Final LRM product and mould design

From the above ring filling calculations, the warpage after cooling resulted in 0.65 %, therefore, the entire design was scaled with this value to ensure a proper fit to the tube. With the resonator and ring dimensions in place, the design is further tailored for IM manufacturing. To this end, draft angles are incorporated in the entire design except for the inner diameter to facilitate demoulding while maintaining a large contact area with the pipe. Furthermore, all sharp corners are rounded to reduce internal stresses. Lastly, a cantilever-snap fit with a plug diameter of 4 mm is added and the LRM part design is further tailored for IM. These changes lead to the LRM design shown in Fig. 4a, for which a final resonator eigenfrequency of 571 Hz is obtained. To facilitate the moulding process, a 5 mm diameter runner is designed, and a submarine gate is selected. This gate type enables automatic part-gate separation during demoulding caused by the undercut which is present. The mould design includes two part

cavities, with the parting plane positioned at the product's center (Fig. 4b).

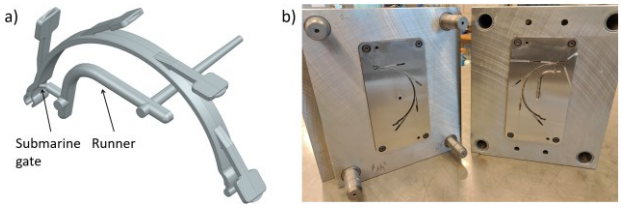

Figure 4: a) Final LRM and runner design, b) both cavity inserts positioned in the mould.

4.4 LRM manufacturing

The moulding is performed using a single screw electrical DEMAG ERGOTECH IntElect 50/330-100 IM machine. The maximal mould clamping force is 500 kN, while a 22 mm horizontal screw with a L/D ratio of 20 is used. The mould temperature is regulated using a EURO CHILLER 3FLOWS P 612/90 controller. The primary process parameters are listed in Table 3. During manufacturing, a cycle time of 21 seconds is maintained. To assemble the LRM, sixteen ring sections (Fig. 5a) are added to the tube (Fig. 5b), leading to 8 full ring additions with a intermediate spacing of 25 mm.

Table 3: Main IM process parameters.

Dosing volume [cm3]	16.3
Switch over point [cm3]	4.4
Melt temperature [°C]	240
Mould temperature [°C]	70
Packing pressure [MPa]	60
Packing time [s]	5
Cooling time [s]	20
Volumetric injection rate [cm3/s]	26.6

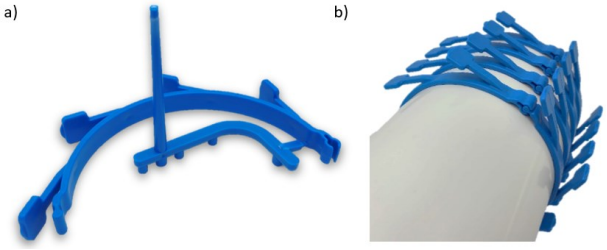

Figure 5: a) Manufactured LRM ring with runner, b) LRM rings assembled to the aluminium pipe.

5. RESONATOR AND LRM PERFORMANCE PREDICTIONS

The resonator eigenfrequencies and the LRM stop bands are predicted using the corresponding resonator and 25 mm UC FE-models. To this end, the manufacturing process-informed toolchain as proposed in [7] is used. This allows to account for process induced shrinkage and density during the predictions by transferring the deformed Boundary Layer Mesh (BLM) with distributed material density obtained from the IM simulation to structural FE. Therefore, an in-house material property mapping routine is used, in which the Scattered Interpolation [9] method is implemented in MATLAB. This method employs Delaunay triangulation to construct an interpolation function over the IM mesh. The material properties on the FE mesh are then computed using linear interpolation, ensuring smooth transitions. From the resonator FE model, the eigenfrequencies are calculated. Next, the resonator mesh is mated to host-structure for stop band calculation.

5.1 Deformed geometry and density distribution

With the final LRM, runner and gate design in place, a filling, packing and warpage simulation is conducted. Fig. 6 shows the resulting displacement of the base ring and resonators, along with the density distribution. The total displacement due to shrinkage and warpage consists of the displacement in the base ring and the displacement of the individual resonators. The ring inner diameter decreases which was already accounted for in the design to ensure a proper fit to the pipe. The resonator shrinkage is expected to lead to an increased eigenfrequency. Additionally, differences in shrinkage between the different resonators (res. 1-4) also result from the non-uniform shrinkage. The density distribution shows a decreased density at the resonator feet, in line with the shrinkage results from the manufacturability assessment in section 4.2. This density decrease at the

feet becomes more pronounced with increasing distance from the gate, as the extended flow length makes the shrinkage compensation during the packing phase more difficult. Overall, the resulting net density is 1030 kg/m^3, compared to the datasheet value of 1050 kg/m^3. The total predicted part mass is calculated to be 7.953 g.

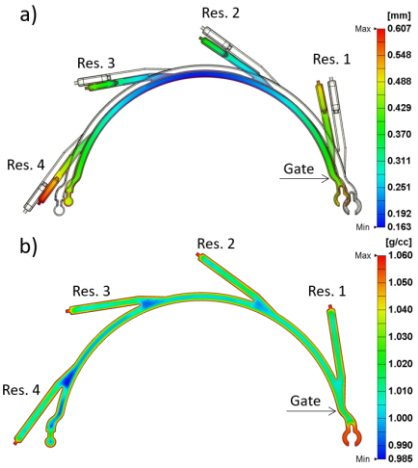

Figure 6: a) Displacement [mm] (deformation x10) and b) density distribution [g/cc] within the LRM ring obtained from IM simulation.

5.2 Eigenfrequency and stop band predictions

The resonator eigenfrequencies for an entire ring section are predicted in Siemens Simcenter using solution 103. A fixed boundary condition is applied on the inner and outer surfaces of the ring. Tab. 4 lists the predicted resonator eigenfrequencies in accordance with the numbering of Fig. 6.

Table 4: Resonator eigenfrequencies obtained form manufacturing-informed predictions.

Resonator 1 [Hz]	579.71
Resonator 2 [Hz]	579.71
Resonator 3 [Hz]	579.73
Resonator 4 [Hz]	580.60

As expected from the calculated model shrinkage and density distribution, all eigenfrequencies increase with respect to the original 571 Hz obtained after drafting. Again, only small differences appear among the resonators individually. This is expected, as the overall displacement and density distribution in the resonator cross-sections are uniform. Since the lower density of resonator 4 occurs in the resonator base, it does not significantly influence the resonator eigenfrequency.

Figure 2 compares the calculated dispersion curves for the bare and LRM case. For the bare tube, the cut-off frequency of the ovalling mode is at 582Hz. Due to the addition of the resonators and their interaction with the ovalling and bending wave, two new cut-on frequencies appear at 499.8 Hz and 665.9 Hz. The obtained stopband for the ovalling mode is (indicated in red) situated between 562.3 Hz and 665.9 Hz. A second bandgap is obtained in the bending wave branch between 562.3 Hz and 579.8 Hz result.

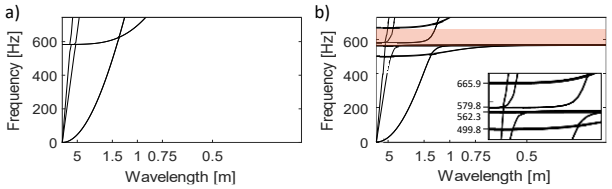

Figure 2: Obtained dispersion diagrams for the a) bare and b) LRM pipe.

6. LRM VALIDATION

For the LRM pipe with 8 fully assembled rings, the forced response is measured. The impact locations are chosen around the circumference, in front of the LRM rings while the response is captured behind the resonator ring additions (Fig. 13). To evaluate the influence of both the clamping and the mass of the rings on the pipe's response, both required to fasten the resonators to the pipe, an non-resonant ring case is created using the rings but removing the resonators, called the non-resonant ring case.

For the non-resonant ring case, the addition of the rings to the pipe clearly lowers the frequency of the first mode (ovalling) while only slightly influencing the second mode (bending). When adding the LRM rings, a clear decrease in the response between 553 Hz and 655 Hz is caused by the resonant effect of the LRM. This is in fair agreement with the predicted stop band between 562.3 Hz and 665.9 Hz. Furthermore, the first peak in the LRM curve around 500 Hz corresponds to the cut-on frequency of the ovalling mode in the LRM dispersion curve. Here the tube's and resonators' motion are in phase. After the stop band, a peak is observed in the FRF

around 655 Hz, which corresponds to the ovalling cut-on frequency after the stop band in the dispersion curve.

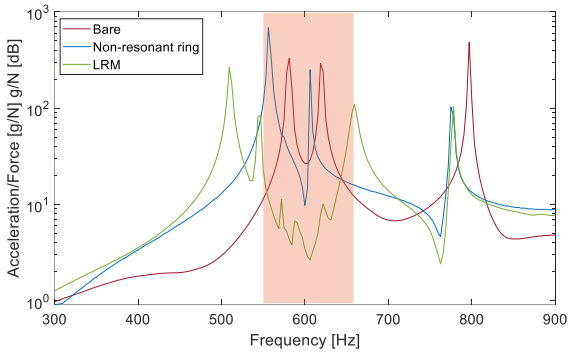

Figure 3: Measured vibration response of the bare, equivalent mass and LRM pipe.

7. CONCLUSION

IM allows for mass-manufacturing of LRM resonators whereas the incorporation of IM process simulation outcomes in the LRM performance predictions has been shown to reduce the off-design performance of resonators. This work builds upon these findings and demonstrates the design and manufacturing of a ready-to-use LRM solution. More specifically, the first ovalling mode of an aluminium pipe is experimentally determined, based on which an LRM ring with four resonators is designed for vibration treatment. To this end, three different resonator designs are found using parameter optimization, whereafter the manufacturability of the designs has been assessed using IM simulations. The final LRM is manufactured and experimentally characterized. The final LRM stop band is predicted using manufacturing-informed predictions, and good agreement is found with experimental pipe response measurements. The successful mass-manufacturing of a ready-to-use LRM with targeted as-manufactured performance facilitates the integration of LRMs in larger-scale designs and paves the way for mass-manufacturable lightweight products with superior NHV performance by design.

8. ACKNOWLEDGMENTS

The research of K. Steijvers (fellowship no. 1S63423N) and L. Van Belle (fellowship no. 1254325) is funded by a grant from the Research Foundation – Flanders (FWO). The Research Foundation Flanders (FWO) and São Paulo Research Foundation-Brazil (FAPESP) are gratefully acknowledged for their support through the bilateral research cooperation project (FWO no. G0F9922N, FAPESP no. 21/05510-3). This research was partially supported by Flanders Make, the strategic research centre for the manufacturing industry.

9. REFERENCES

[1] M. I. Hussein, et al., "Dynamics of phononic materials and structures: Historical origins, recent progress, and future outlook," *Appl. Mech. Rev.*, vol. 66, no. 4, Jul. 2014, doi: 10.1115/1.4026911.

[2] C. Claeys, et al., "On the potential of tuned resonators to obtain low-frequency vibrational stop bands in periodic panels," *J. Sound Vib.*, vol. 332, no. 6, pp. 1418–1436, Mar. 2013, doi: 10.1016/j.jsv.2012.09.047.

[3] X. Wu, et al., "Perspective of additive manufacturing for metamaterials development," Aug. 12, 2019, *Institute of Physics Publishing*. doi: 10.1088/1361-665X/ab2eb6.

[4] E. Deckers *et al.*, "Locally resonant vibro-acoustic metamaterials: applications at KU Leuven," in *DAGA 2021, (90-93)*,

[5] K. Steijvers, et al., "Injection moulding of resonators for locally resonant metamaterial production," in *AIP Conference Proceedings: The 2nd international symposium on plastics technology*, Aachen, Germany: American Institute of Physics, May 2024. doi: 10.1063/5.0192336.

[6] J. Yu, et al., "Mass production applicable locally resonant metamaterials for NVH applications," in *Proceedings of the 26th International Congress on Sound and Vibration, ICSV 2019*.

[7] K. Steijvers, et al., "Incorporating Manufacturing Process Simulations to Enhance Performance Predictions of Injection Moulded Metamaterials," *J. Vib. Eng. Technol. 2023*, vol. 1, pp. 1–13, Oct. 2023, doi: 10.1007/S42417-023-01159-1.

[8] A. Nateghi, et al., "Design and experimental validation of a metamaterial solution for improved noise and vibration behavior of pipes," *J. Sound Vib.*, vol. 455, pp. 96–117, Sep. 2019, doi: 10.1016/j.jsv.2019.05.009.

[9] I. Amidror, "Scattered data interpolation methods for electronic imaging systems: a survey," 2002, doi: 10.1117/1.1455013.